

CETCAM: Camera-Controllable Video Generation via Consistent and Extensible Tokenization

Zelin Zhao¹ Xinyu Gong² Bangya Liu³ Ziyang Song⁴ Jun Zhang²
 Suhui Wu² Yongxin Chen¹ Hao Zhang²

¹Georgia Institute of Technology ²ByteDance

³University of Wisconsin–Madison ⁴The Hong Kong Polytechnic University



Figure 1. **Camera-controlled Video Generation.** Our framework synthesizes **dynamic, geometry-consistent** scenes across diverse domains, including human face, animal motion, and natural environments. It allows accurate camera control across wide viewpoints, with full 360° orbit motion shown in the last example. Please refer to the project page for videos, code and pre-trained models.

Abstract

Achieving precise camera control in video generation remains challenging, as it often relies on camera pose annotations that are difficult to scale to large, dynamic datasets and are frequently inconsistent with depth estimation, leading to train–test discrepancies. We introduce CETCAM, a camera-controllable video generation framework that eliminates the need for camera annotations through consistent and extensible tokenization. CETCAM incorporates recent advances in geometry foundation models (e.g., VGGT) to estimate depth and camera parameters, converting them into unified, geometry-aware tokens that are seamlessly integrated into a pretrained video diffusion backbone via lightweight context blocks. Trained in two progressive phases, CETCAM learns robust cam-

era controllability from diverse raw videos and refines fine-grained visual quality on curated high-fidelity data. Extensive experiments across multiple benchmarks demonstrate state-of-the-art geometric consistency, temporal stability, and visual realism. Moreover, CETCAM exhibits strong adaptability to additional control modalities (e.g., inpainting or layout), highlighting its flexibility beyond camera control. The project page is available at https://sjtuytc.github.io/CETCam_project_page.github.io/.

1. Introduction

Recent advances in video diffusion models (VDMs) have greatly improved visual quality and temporal coherence

across diverse domains [22, 27]. However, precise camera control in dynamic scenes remains a major challenge. Existing large-scale video foundation models, such as Wan [22] and CogVideoX [27], often lack explicit 3D understanding and struggle to manipulate viewpoints reliably. As a result, generating videos with consistent multi-view geometry or user-specified camera motion remains highly non-trivial—let alone combining camera control with other conditioning tasks such as object manipulation or inpainting.

Earlier attempts to address this challenge can be grouped into three broad categories. Training-free approaches [7, 35] manipulate pretrained diffusion models via latent-space optimization or editing. While simple to deploy, these methods are typically unstable and fail to generalize to unseen scenes or complex camera trajectories [4]. Novel-view synthesis (NVS) methods [16, 17, 20, 28] introduce explicit 3D constraints by reconstructing and rendering scene geometry. However, they are largely limited to static environments and cannot effectively model dynamic motion or long-range temporal consistency. More recently, several camera-controllable diffusion frameworks such as ReCam-Master [2] and Gen3C [18] have extended diffusion-based video generation with explicit camera conditioning, often by constructing or rendering intermediate 3D representations. While these approaches demonstrate improved viewpoint control, they typically train on annotated camera poses or separately estimated depth supervision. Moreover, their designs are specialized for camera motion only—making them difficult to extend to other conditioning modalities such as sketch or layout. Furthermore, the concurrent work Uni3C [4] explores a similar idea of integrating camera control into video diffusion models but often suffers from local distortions and geometric misalignment due to inaccurate 3D consistency between estimated depth and pose signals.

To overcome these limitations, we propose **Consistent and Extensible Tokenization (CETCAM)** for controllable camera-driven video generation. Our model builds upon recent advances of the Visual Geometry Grounded Transformer (VGGT) [23], jointly predicting camera poses and depth maps, followed by point-based reprojection that generates renderings and masks that encode view-dependent geometry. These signals are then embedded into compact, geometry-aware camera tokens, enabling explicit yet annotation-free camera conditioning within the diffusion process. To integrate with large-scale video diffusion backbones, we introduce CETCAM context blocks that serve as plug-in modules to the frozen base video diffusion model, allowing seamless conditioning without retraining the base model. As shown in Figure 1, our framework enables precise camera control across diverse scenes while preserving geometric consistency and visual fidelity.

Beyond camera control, our framework is inherently extensible. Inspired by the VACE architecture [11],

CETCAM integrates seamlessly with additional control modalities, supporting unified compositional generation under multiple types of conditioning. This design allows CETCAM to go beyond camera control and serve as a general interface for combining geometric and semantic guidance in controllable video generation.

Extensive experiments demonstrate that CETCAM significantly outperforms prior camera-controllable video generation methods across multiple benchmarks. Compared with Uni3C [4], our approach achieves overall VBench [10] score improvements of +3.09%, +2.70%, and +2.88% on the Uni3C-OOD-Challenging [4], CameraBench [15], and our newly collected HoIHQ benchmark, respectively. The HoIHQ dataset is a high-fidelity human-object interaction benchmark specifically curated for evaluating camera-controllable video generation in dynamic and realistic settings. Human evaluation results further confirm the superiority of our method, with perceptual scores of 90.3, 91.5, and 93.4 on the respective benchmarks—an average gain exceeding 6% over the previous best. Additionally, CETCAM achieves more accurate and stable camera trajectory following, reducing pose errors by over 15% across all benchmarks. Moreover, the framework preserves strong camera controllability and high generative quality while remaining extensible to additional control modalities.

Our **main contributions** are summarized as follows:

1. We propose the CETCAM camera tokenizer for controllable viewpoint video generation, where it jointly predicts depth maps and camera parameters, and performs point-based reprojection to generate renderings and masks that encode view-dependent geometry. These signals are further embedded into camera tokens, eliminating the need for explicit camera labels and enabling robust training across diverse real-world videos.
2. We introduce an extensible controlled video generation framework that integrates the proposed camera tokens with additional conditioning modalities. The design enables seamless compositional control—combining camera motion with inputs such as inpainting or grayscale cues—while preserving the expressive and generative capacity of the base diffusion model. This establishes a scalable, token-based conditioning interface applicable across diverse control types.
3. Through extensive experiments across multiple benchmarks, we demonstrate that our method achieves accurate camera control, maintaining strong temporal and geometric consistency across diverse scenes. It also preserves high visual fidelity compared to recent baselines and further validates the framework’s extensibility when integrated with other controllable generation modalities.

2. Related Works

Video Generation with Camera Control. Camera-controllable video generation has recently moved from implicit viewpoint conditioning to explicit 3D-aware control. Training-free methods are often limited in quality or extensibility [7, 35]. Most video novel view synthesis (NVS) methods are limited to static scenes and cannot model dynamic motions [16, 17, 20, 28, 34]. Gen3C [18] introduces the idea of constructing and rendering a 3D cache as a conditioning signal, outperforming approaches that directly inject camera poses [6]. Similar 3D rendering-based mechanisms are adopted in recent works [1, 4, 6, 8, 26], where depth or point-based re-projections are used to inject camera pose into the diffusion backbone. EPiC [26], though architecturally distinct from ours, is trained on a very small dataset and built upon a weaker base model (CogVideoX-5B [27]), leading to inferior visual fidelity. The closest concurrent work, UNI3C [4], depends on camera annotations and adopts mismatched depth estimators during training (SfM [19]) and testing (Depth Pro [3]). Our method differs by learning directly from raw dynamic videos without requiring annotation, achieving consistent geometric grounding, better visual quality and higher extensibility.

Controllable Video Synthesis and Editing. Beyond viewpoint control, a parallel line of work focuses on controllable video diffusion models that accept diverse user controls. VideoCrafter2 [5] and VideoComposer [24] extends text-to-video diffusion models with various motion control techniques, while ControlVideo [31] adapts image-control modules to preserve temporal consistency. VACE [11] is a unified model that extends ControlNet-style conditioning to videos, enabling versatile and composable video generation and editing tasks within a single framework. MotionDirector [32] does not address the more challenging problem of controlling camera angle changes, which remains nontrivial. FullDiT [12], which is a recent concurrent work without available pre-trained models or code, conducts various controls including camera control.

Geometry-grounded Models. Recent works focus on learning geometry from visual data through feed-forward architectures that infer depth, camera pose, and 3D structure directly from images or videos. VGGT [23] introduced a unified backbone predicting dense geometry and camera parameters from unconstrained inputs. Its follow-ups further extend this paradigm: π^3 [25] removes the reference-view bias with a permutation-equivariant design, ViPE [9] adapts geometry estimation to dynamic video scenes with large-scale annotated data, and MapAnything [13] unifies diverse 3D reconstruction tasks into a single transformer model. These advances demonstrate a clear trend toward scalable and consistent visual geometry learning.

3. Methodology

Our objective is to develop a controllable video generation framework that enables precise manipulation of camera viewpoints in complex and dynamic scenes, without requiring explicit camera annotations. The design of our method is guided by two key principles: (a) **Consistency** — The model must leverage consistent camera poses and depth maps while maintaining coherence between the training and testing regimes; (b) **Extensibility** — the framework should readily extend to additional forms of control, such as inpainting or sketch guidance [11]. Meanwhile, the system should be computationally efficient to train while preserving the expressive power of the underlying generative backbone. An overview of the proposed architecture is shown in Figure 2. Our architecture is instantiated under the image-to-video (I2V) setting following UNI3C [4].

3.1. CETCAM Tokenizer

As illustrated in Figure 2(a), the CETCAM Tokenizer transforms raw, in-the-wild training videos (during training) or a reference frame with corresponding camera poses (during inference) into compact, geometry-aware representations that encode visual content and camera motion.

Training-time Tokenization. Unlike prior controllable video generation baselines [4] that require explicit camera annotations, we employ the Visual Geometry Grounded Transformer (VGGT) [23] to estimate both depth maps and camera parameters directly from raw videos. Given an input video sequence $\{I_t\}_{t=1}^T$ with T frames, we first predict per-frame depth maps $\{\mathbf{D}_t\}_{t=1}^T$, corresponding camera extrinsics $\{\mathbf{E}_t\}_{t=1}^T$ and intrinsics $\{\mathbf{K}_t\}_{t=1}^T$ via a pre-trained frozen VGGT [23] model:

$$\{\mathbf{D}_t, \mathbf{E}_t, \mathbf{K}_t\}_{t=1}^T = \text{VGGT}^{(\text{frozen})}(\{I_t\}_{t=1}^T). \quad (1)$$

This estimation ensures that the predicted depths and poses are geometrically aligned across frames and uniform across diverse training datasets, overcoming inconsistencies typically found in camera label annotations [23]. After that, a **point cloud reprojection** procedure is introduced to project the first frame’s pixels into other frames, generating a rendering and a mask. We refer the readers to Figure 3 for examples of renderings. Inferring both a rendering and a mask is central to many concurrent approaches, including inpainting-based video generation [4, 8] and generation conditioned on anchor videos [26]. Specifically, the depth map \mathbf{D}_1 and camera intrinsics \mathbf{K}_1 of the first frame are used to back-project each pixel $\mathbf{y}_1^{(i)} = [u^{(i)}, v^{(i)}, 1]^\top$ in the image plane of I_1 into 3D space, yielding a 3D point $\mathbf{X}^{(i)}$:

$$\mathbf{X}^{(i)} = \mathbf{D}_1(\mathbf{y}_1^{(i)}) \mathbf{K}_1^{-1} \mathbf{y}_1^{(i)}, \quad \mathbf{X}^{(i)} \in \mathbb{R}^3. \quad (2)$$

We then map $\mathbf{X}^{(i)}$ into the coordinate frame of I_t via the predicted extrinsics $\mathbf{E}_t = [\mathbf{R}_t | \mathbf{T}_t]$ and re-project it onto

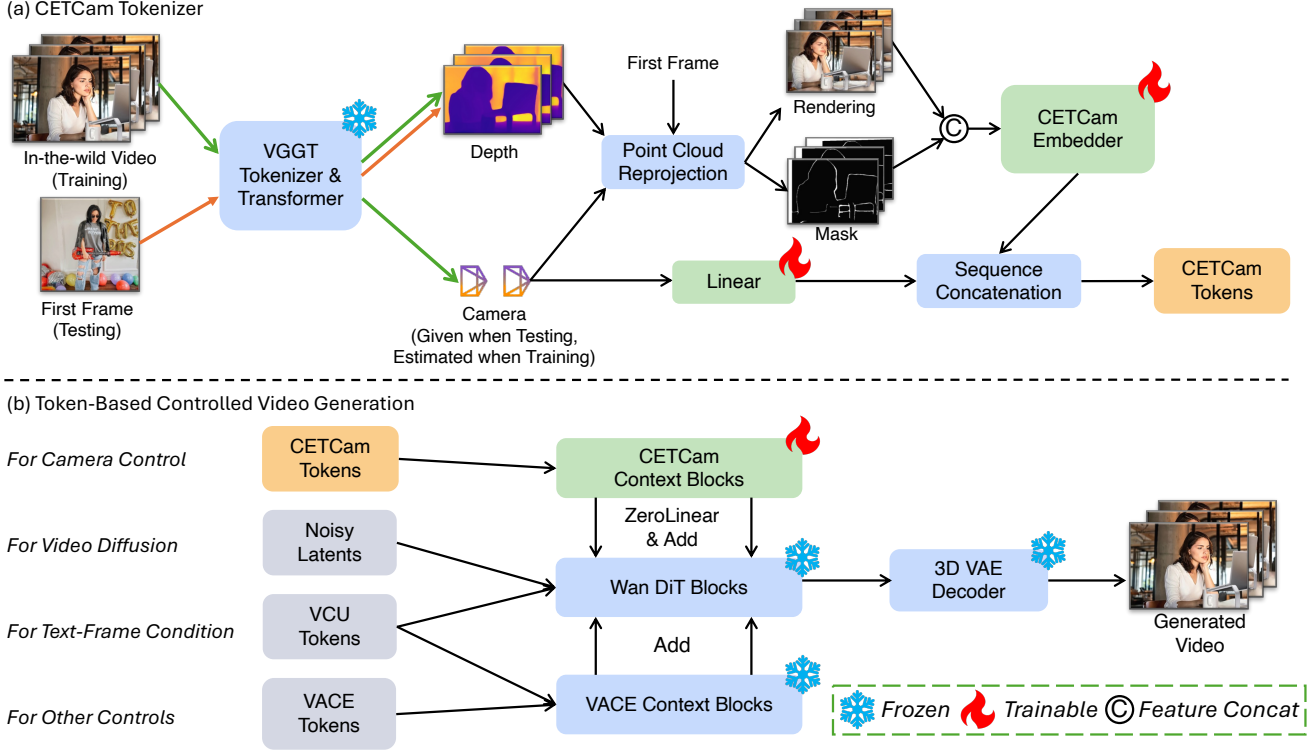


Figure 2. **Overview of CETCAM I2V generation framework.** (a) *CETCAM Tokenizer*: Given an in-the-wild training video or a test-time frame input, the frames are processed by VGGT [23] to predict the depth maps. In training, camera poses are also estimated. Predicted depths and camera poses are used for point cloud reprojection to generate renderings of the first frame and corresponding masks. Renderings, masks, and camera poses are embedded and fused to produce CETCAM tokens. (b) *Token-Based Controlled Video Generation*: We leverage various tokens with rich and diverse functions via different tokens, including CETCAM tokens, noisy latents, VCU tokens, and VACE tokens [11]. CETCAM tokens are consumed in learnable CETCAM context blocks, which were connected to pre-trained Wan DiT blocks [22] with zero linear and add functions [4]. Other tokens are further processed by VACE context blocks and Wan DiT blocks. Finally, the output tokens are decoded through a 3D VAE to generate a video [22]. More details can be found in Sections 3.1 and 3.2.

the image plane of I_t using \mathbf{K}_t :

$$\tilde{\mathbf{y}}_t^{(i)} \sim \mathbf{K}_t(\mathbf{R}_t \mathbf{X}^{(i)} + \mathbf{T}_t). \quad (3)$$

The projected coordinates $\tilde{\mathbf{y}}_t^{(i)}$ define the image-plane sampling locations in frame I_t . By assigning each $\tilde{\mathbf{y}}_t^{(i)}$ the color value from its corresponding 3D point $\mathbf{X}^{(i)}$ in I_1 , we obtain a synthesized view \tilde{I}_t —referred to as the **rendering**. Meanwhile, we construct a binary visibility **mask** $\mathbf{M}_t \in \{0, 1\}^{H \times W}$ for each frame based on point correspondences and occlusion checks, retaining only pixels whose projections $\tilde{\mathbf{y}}_t^{(i)}$ are traced from the reference frame I_1 , where H and W are height and width, respectively:

$$\mathbf{M}_t(\tilde{\mathbf{y}}_t^{(i)}) = \begin{cases} 1, & \text{if } \tilde{\mathbf{y}}_t^{(i)} \text{ is visible and traced from } I_1, \\ 0, & \text{otherwise.} \end{cases} \quad (4)$$

The resulting mask \mathbf{M}_t helps preserve regions reprojected from I_1 while filtering out occluded or unmatched areas.

The renderings \tilde{I}_t and corresponding masks \mathbf{M} are concatenated along the channel dimension and processed by a learnable CETCAM Embedder $\mathcal{E}_{\Theta_{emb}}$. The CETCAM Embedder follows the same architecture as the Wan video embedder [11, 22]. We get the encoded rendering-mask as $\mathbf{z}_t^{(rm)} \in \mathbb{R}^{T \times H \times W \times d}$ where d is the feature dimension:

$$\mathbf{z}_t^{(rm)} = \mathcal{E}_{\Theta_{emb}} \left(\text{Concat}_{\text{feat}}(\tilde{I}_t, \mathbf{M}_t) \right). \quad (5)$$

The embedding weights corresponding to \tilde{I}_t are initialized from the Wan video embedder [11, 22], and the remaining weights corresponding to the mask \mathbf{M}_t are zero-initialized.

Furthermore, we encode camera poses to augment the render-mask tokens $\mathbf{z}_t^{(rm)}$. Following VGGT [23], we represent the camera parameters using a quaternion-based concise form of the extrinsic and intrinsic matrices, denoted by $\mathbf{g}(\mathbf{E}_t, \mathbf{K}_t) = [\mathbf{q}_t, \mathbf{T}_t, \mathbf{f}_t]$, where $\mathbf{q}_t \in \mathbb{R}^4$, $\mathbf{T}_t \in \mathbb{R}^3$, $\mathbf{f}_t \in \mathbb{R}^2$ are the rotation quaternion, the translation vector, and the field of view, respectively. These vectors are concatenated in the feature dimension and passed through a linear

layer to get a camera parameter embedding $\mathbf{z}_t^{(\text{pr})} \in \mathbb{R}^d$, while $\mathbf{W}^{(\text{pr})}$ and $\mathbf{b}^{(\text{pr})}$ are learnable linear weights:

$$\mathbf{z}_t^{(\text{pr})} = \mathbf{W}^{(\text{pr})} \text{Concat}(\mathbf{q}_t, \mathbf{T}_t, \mathbf{f}_t) + \mathbf{b}^{(\text{pr})}. \quad (6)$$

Finally, we concatenate $\mathbf{z}_t^{(\text{pr})}$ with the visual tokens $\mathbf{z}_t^{(\text{rm})}$ along the sequence dimension to form the final **CETCAM token** $\mathbf{z}_t^{(\text{CETCAM})} \in \mathbb{R}^{(THW+1) \times d}$ that jointly encodes visual content and camera geometry:

$$\mathbf{z}_t^{(\text{CETCAM})} = \text{Concat}_{\text{seq}}(\mathbf{z}_t^{(\text{rm})}, \mathbf{z}_t^{(\text{pr})}). \quad (7)$$

Test-time Tokenization. During inference, the model takes a reference frame I_1 as input, along with the camera parameters for all testing frames $\{\mathbf{E}_t, \mathbf{K}_t\}_{t=1}^T$. A single-view depth map \mathbf{D}_1 corresponding to the reference frame is estimated using VGGT [23]. A 3D point cloud is then derived using the back-projection formula (Equation (2)). After that, renderings, masks, and CETCAM tokens are derived following Equations (3), (4), (6) and (7).

3.2. Token-Based Controlled Video Generation

As shown in Figure 2 (b), building upon the frozen pre-trained Wan DiT blocks, we introduce a token-based conditioning mechanism that integrates CETCAM tokens with other control modalities in a unified latent space. In particular, our generation pipeline operates on four token types: (1) CETCAM *tokens* carrying camera poses and 3D geometry context. (2) *Noisy latents*, which are the initial Gaussian noises, are iteratively denoised during the diffusion process. (3) *Visual Condition Unit (VCU) tokens* represent the prompt, first frame, and mask. Here, the mask indicates all pixels to be modified by either the CETCAM control or the VACE control. Noisy latents and VCU tokens already exist in the base Wan model. (4) *VACE tokens* [11] encoding versatile external conditions such as layout or sketch. VACE tokens are not added if only the camera control is added.

These tokens are integrated into the base video diffusion model [22]. Specifically, the CETCAM tokens are processed by a set of learnable **CETCAM Context Blocks**. Their outputs are projected through zero-initialized linear layers to align the feature dimensions with those of the Wan DiT blocks. The resulting embeddings are then added to the Wan DiT blocks [22], except for the token corresponding to the camera, which is excluded before the addition. In parallel, noisy latents and VCU tokens are injected into the Wan DiT blocks. Frozen VACE context blocks are also added to the Wan DiT blocks, conditioned jointly on the text embeddings and VACE tokens.

3.3. Dataset Construction and Training Strategy

Training data plays a pivotal role in building effective video generative models [22]. A key advantage of CETCAM is

that it can be trained directly on raw videos without requiring any camera pose annotations. We adopt a two-phase training strategy to progressively develop camera control capability while improving the generative quality.

In Phase One, we focus on learning general camera control from large-scale, diverse data. We collect a dataset of approximately 330K online videos and apply two filtering steps: (1) removing static-camera videos based on camera motion estimated by VGGT, and (2) discarding videos with low aesthetic quality measured by VBench [10]. After filtering, the resulting dataset contains roughly 100K videos. We also incorporate VACE-Benchmark to preserve the controllability of VACE tokens. Further details of this collection and filtering process are provided in Section 6.

In Phase Two, we emphasize fine-grained generation quality using a smaller, high-fidelity dataset. The training data consists of the training split of CameraBench [15], the I2V training set of VACE-Benchmark and our collected HoIHQ benchmark, totaling about 3K high-quality videos. The HoIHQ benchmark is generated from a state-of-the-art video foundation model Kling 2.5 [21], while images are our collected high quality human object interaction (HoI) images (see dataset construction details in Section 7).

For both phases, the training parameters are the same (marked with a fire symbol in Figure 2). Besides, the training targets are also the same, where we minimize the standard video flow matching loss [22]:

$$\mathcal{L}_{\text{vel}} = \mathbb{E}_{t, \mathbf{x}_0, \mathbf{x}_1, c} \left[\left\| \mathbf{v}_\theta(\mathbf{x}_t, t, c) - (\mathbf{x}_1 - \mathbf{x}_0) \right\|_2^2 \right], \quad (8)$$

where $\mathbf{x}_0 \sim \mathcal{N}(\mathbf{0}, \mathbf{I})$ is a Gaussian noise latent, $\mathbf{x}_1 = \mathcal{E}(I)$ is the encoded clean latent from the 3D VAE encoder, and $\mathbf{x}_t = (1-t)\mathbf{x}_0 + t\mathbf{x}_1$ interpolates between them at timestep $t \in [0, 1]$. The model $\mathbf{v}_\theta(\mathbf{x}_t, t, c)$ predicts the velocity field conditioned on c , which includes the text embedding and the input frame condition. Through this unified objective, CETCAM progressively learns both visual fidelity and geometric consistency across training phases, which ensures stable optimization and seamless alignment between camera motion and scene dynamics.

4. Experiments

4.1. Experimental Setups

Training and Inference Configurations. We adopt 14B Wan-I2V Diffusers 2.1 [22] as our base model. CETCAM context blocks contain 20 external DiT layers, while the total number of trainable parameters is around 1B. We scale multi-resolution videos to a resolution of 587×587 with a total of 77 frames, at an FPS of 16. Since the Wan model tokenizes videos into spatiotemporal patches before sequential processing, the total number of tokens (i.e., overall spatiotemporal resolution) primarily determines the model’s

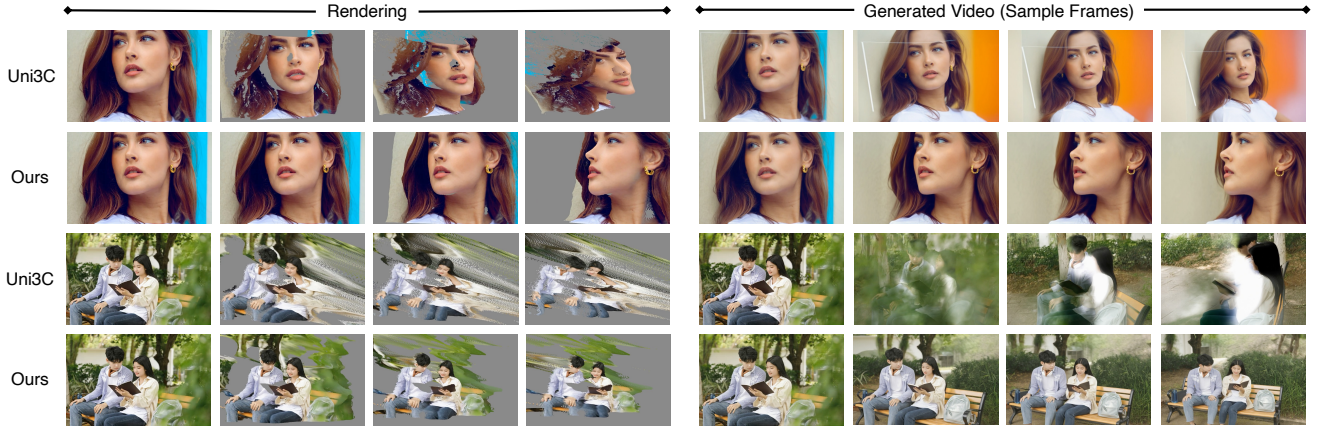


Figure 3. **Comparison with the closest concurrent work UNI3C [4].** *Left:* UNI3C renderings fail to accurately follow the intended camera motion and exhibit geometric distortions and outliers due to inconsistent 3D estimation. *Right:* These inaccuracies in renderings lead to spatial misalignment and visible artifacts in the generated videos of UNI3C, while our generated videos do not exhibit these artifacts.

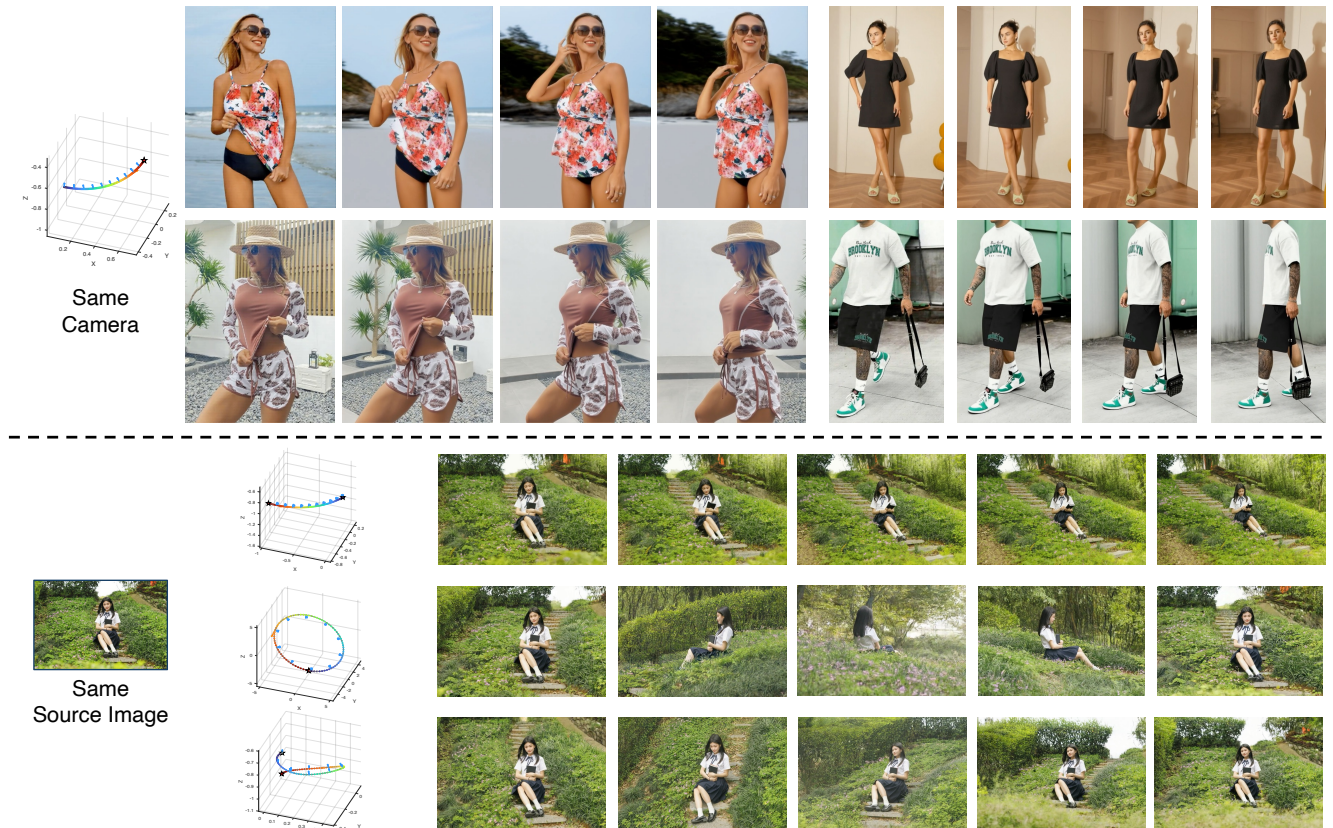


Figure 4. **Camera control results.** *Top:* Four videos generated under the same camera trajectory (source images omitted for brevity). *Bottom:* Results with the same source image but different camera trajectories, illustrating consistent control across four distinct motions.

input size. For each training phase, the learning rate is linearly warmed up to 10^{-5} over the first 1K steps and then kept constant. Phase I training runs for 100K steps, while Phase II training runs for an additional 10K steps. The entire training process takes approximately one week on 32 H100 GPUs. Text prompts are generated with Tar-

sier2 [29] using a simple descriptive query. Inference is performed with classifier-free guidance set to $c_{\text{CFG}} = 5.0$. The generated videos last for 5 seconds, for ours and all baselines. To save GPU memory, we adopt Fully Sharded Data Parallel (FSDP) [33] and Sequence Parallelism (SP) [14] on the base model (please refer to Section 9 for details).

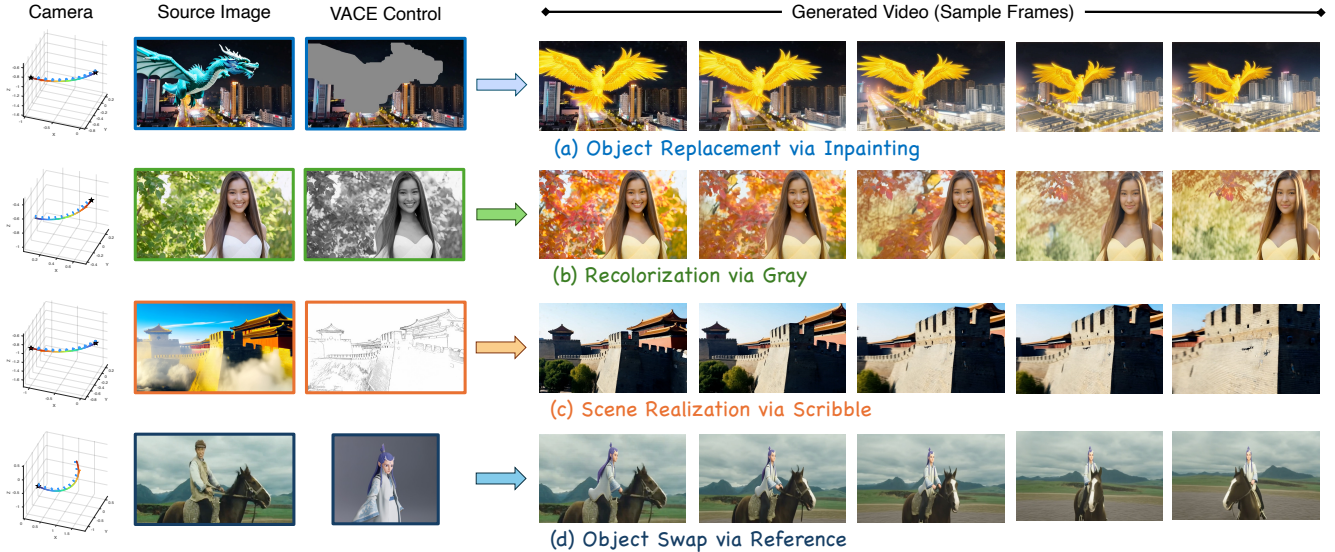


Figure 5. **Extensibility Results.** We show visualization results on controlling camera motion while achieving additional control through VACE [11]. (a) *Object replacement* (with prompt “replace the dragon with a phoenix”) using a source image and a masked image as VACE control, (b) *Recolorization* of a green portrait guided by a gray image control, (c) *Realization* of a virtual scene from a scribble as VACE control, and (d) *Object swap* guided by a provided reference image. Please refer to the supplementary for more demo videos.

	Overall Score	Subject Consistency	Background Consistency	Aesthetic Quality	Imaging Quality	Temporal Flickering	Motion Smoothness	ATE↓	RPE↓	RRE↓	Human Eval↑
UNI3C-OOD-Challenging Dataset [4]											
CameraCtrl [6]	74.35	78.62	83.17	49.22	57.30	86.04	89.78	1.982	0.903	7.412	70.1
SEVA [34]	80.67	85.42	89.35	54.06	63.52	92.74	95.86	1.212	0.562	5.138	81.4
EPiC [26]	78.92	83.04	87.22	52.38	61.47	90.11	93.56	1.486	0.691	6.307	78.6
UNI3C [4]	82.75	88.19	91.03	57.61	66.90	95.40	97.39	1.003	0.425	4.452	84.9
CETCAM (Ours)	85.84	90.92	93.68	60.71	72.84	97.89	99.56	0.812	0.301	3.674	90.3
CameraBench Dataset [15]											
CameraCtrl [6]	75.64	80.33	84.52	49.85	59.04	87.93	91.21	1.864	0.872	7.109	72.4
SEVA [34]	81.23	86.19	89.66	54.71	64.52	93.51	96.22	1.184	0.534	5.024	82.0
EPiC [26]	79.42	84.57	88.12	53.08	62.48	91.02	94.13	1.402	0.648	6.018	79.8
UNI3C [4]	83.42	88.67	90.92	58.16	69.85	96.12	98.03	0.972	0.416	4.321	86.1
CETCAM (Ours)	86.12	91.84	93.54	61.04	73.12	97.96	99.48	0.793	0.286	3.622	91.5
HoIQ Benchmark (Ours)											
CameraCtrl [6]	78.55	82.37	86.94	50.23	65.28	90.14	93.57	1.622	0.753	6.102	75.3
SEVA [34]	82.71	87.84	90.41	54.39	70.26	94.82	97.35	1.041	0.493	4.971	84.2
EPiC [26]	81.05	85.63	88.79	53.18	68.15	92.73	95.64	1.283	0.618	5.762	81.9
UNI3C [4]	84.36	90.03	91.39	55.03	73.50	97.00	99.19	0.941	0.392	4.206	87.8
CETCAM (Ours)	87.24	92.81	93.57	58.62	76.02	98.06	99.58	0.768	0.259	3.414	93.4

Table 1. **Camera-controlled generation results on three benchmarks.** Metrics include VBench [10] scores (overall, subject and background consistency, aesthetic and imaging quality, temporal flickering, motion smoothness), and 3D pose metrics (ATE, RPE, RRE). We additionally report a human evaluation score measuring perceived realism and temporal consistency. Refer to Section 4.3 for more details.

Baselines. We compare with several strong baselines spanning the spectrum of controllable video generation methods: (1) CameraCtrl [6], which conditions video diffusion models on camera poses through depth- or point-based re-projection into the diffusion backbone; (2) SEVA [34], a novel view synthesis framework for static scenes that incorporates structural cues to enhance viewpoint consistency; (3) EPiC [26], a concurrent method employing a 3D

rendering-based conditioning strategy with lightweight re-projection modules to encode camera geometry during generation; and (4) UNI3C [4], another concurrent large-scale approach that leverages 3D re-rendering with provided camera annotations for camera-controllable video generation.

Datasets. During comparison, each method generates videos conditioned on the same input image and camera trajectories for a fair comparison. We use the following three

Variant	Overall \uparrow	ATE \downarrow	RPE \downarrow	Remark
Full CETCAM	86.1	0.79	0.29	All modules enabled
<i>w/ Text-Informed Camera Embedding</i>	85.7	0.91	0.36	Add text-input in camera encoding
<i>Concat CETCAM Context Block Features</i>	83.9	0.95	0.39	Replace "add" with concatenation
<i>Plücker Ray Tokens</i>	84.4	0.92	0.35	Use Plücker ray as camera tokens
<i>w/o Visibility Mask</i>	83.2	1.05	0.45	Don't use visibility mask
<i>w/o Camera Embeddings</i>	85.8	0.90	0.38	Only use the rendering and mask
<i>Inconsistent Train-Test Depth Estimation</i>	84.6	0.90	0.35	Follow UN13C's depth estimation
<i>Annotated Camera Poses</i>	83.7	0.84	0.34	Poses are not consistent with depths

Table 2. **Further Ablation Study on CameraBench [15]**. Each variant disables or replaces a specific design choice in CETCAM.

benchmarks. (1) UN13C-OOD-Challenging [4], designed for out-of-distribution evaluation, which contains source images and texts without paired videos. This dataset includes extreme camera trajectories unseen during training, highlighting each model’s generalization ability. (2) CameraBench [15], which provides balanced, high-quality samples with moderate camera motion and well-calibrated trajectories, focusing on temporal stability and visual realism. (3) Our constructed HoIHQ benchmark, which emphasizes high-fidelity human–object interactions and indoor scenes. For all experiments on HoIHQ, we use the eight predefined camera trajectories released by UN13C [4]; for each source image, eight corresponding videos are generated following these trajectories to assess viewpoint controllability and geometric consistency. We report results on the held-out validation split for both CameraBench [15] and HoIHQ.

4.2. Camera Control Qualitative Results

We visualize our camera control results in Figure 4. The top part shows four videos generated under the same camera trajectory given different source images, demonstrating consistent and geometry-aware viewpoint motion. The bottom part presents results from a single source image with three distinct camera trajectories, where CETCAM accurately follows each prescribed path while preserving scene structure and visual realism. As further illustrated in Figure 3, our method produces geometrically consistent renderings that faithfully follow camera motion, addressing the distortion and misalignment issues in UN13C [4]. These results highlight our model’s strong controllability and temporal coherence across diverse scenes and motion patterns. Besides, as illustrated in the teaser (Figure 1), our framework generalizes across diverse domains and enables wide-range camera manipulation, including full 360° orbit.

4.3. Quantitative Comparisons

We perform quantitative comparisons between our method and the baselines using three sets of evaluation metrics: (1) Visual quality metrics from VBench [10], which assess overall visual fidelity, subject and background consistency, aesthetic quality, imaging sharpness, temporal flickering, and motion smoothness; (2) 3D geometric metrics [4], including Absolute Trajectory Error (ATE), Relative Pose Error (RPE), and Relative Rotation Error (RRE), to evaluate camera pose accuracy and geometric consistency; and (3)

Human evaluation scores (0–10 initial scores rescaled to 0–100), which measure perceived realism and temporal coherence based on the averaged ratings of 30 participants. Each participant evaluated 100 generated videos per model, which typically required about one hour per model.

As shown in Table 1, CETCAM achieves the best overall performance across all benchmarks, outperforming prior methods in both visual and geometric metrics. It demonstrates accurate camera controllability, improved temporal stability, and robust generalization across diverse video domains, with human evaluation further confirming its superior realism, coherence, and perceptual quality.

4.4. Extensibility Results

We evaluate the extensibility of CETCAM under the image-to-video (I2V) setting by integrating our camera tokens with additional conditioning modalities provided by VACE [11]. As shown in Figure 5, CETCAM supports four compositional controls such as object replacement, recolorization, scene realization, and object swap, achieving coherent generation under dynamic camera motion. These results highlight that the proposed token-based design scales effectively and remains highly compatible with multi-modal conditioning, enabling seamless integration of camera control with appearance- or structure-level guidance. Quantitative comparisons are in the supplementary (Section 8).

4.5. Further Ablation Studies

We conduct detailed ablations on the validation split of CameraBench [15] to ablate the full CETCAM model, as summarized in Table 2. Replacing additive feature fusion with concatenation or substituting our quaternion-based camera tokenization (following VGGT [23]) with Plücker ray tokens both degrade performance, confirming the benefit of our token and context block design. Removing visibility masks leads to lower visual quality and higher geometric errors, highlighting their importance in filtering occluded regions. Incorporating text-informed camera embeddings [11] does not lead to further improvement, likely because text–camera alignment introduces additional semantic ambiguity and optimization complexity beyond the scope of pure geometric control. Finally, using annotated camera poses or inconsistent depth estimators [4] results in reduced consistency between geometry and motion, validating our design choice of learning from geometry grounded estimations in a unified and consistent manner.

5. Conclusions

We presented CETCAM, a geometry-grounded framework for controllable video generation that enables precise camera manipulation without requiring annotated camera poses. By leveraging depth and pose estimation from geometry foundation models, our method learns from raw dynamic

videos and integrates seamlessly with pretrained diffusion backbones through token-based conditioning. Extensive experiments demonstrate that CETCAM achieves superior geometric consistency, controllability, and visual realism compared to recent baselines, while remaining extensible to additional control mechanisms such as layout or inpainting. We hope this work provides a new foundation for unified and geometry-aware controllable video generation.

References

- [1] Sherwin Bahmani, Ivan Skorokhodov, Guocheng Qian, Aliaksandr Siarohin, Willi Menapace, Andrea Tagliasacchi, David B Lindell, and Sergey Tulyakov. Ac3d: Analyzing and improving 3d camera control in video diffusion transformers. In *CVPR*, pages 22875–22889, 2025. 3
- [2] Jianhong Bai, Menghan Xia, Xiao Fu, Xintao Wang, Lianrui Mu, Jinwen Cao, Zuozhu Liu, Haoji Hu, Xiang Bai, Pengfei Wan, and Di Zhang. Recammaster: Camera-controlled generative rendering from a single video, 2025. 2
- [3] Aleksei Bochkovskii, Amaël Delaunoy, Hugo Germain, Marcel Santos, Yichao Zhou, Stephan R. Richter, and Vladlen Koltun. Depth pro: Sharp monocular metric depth in less than a second. In *International Conference on Learning Representations*, 2025. 3
- [4] Chenjie Cao, Jingkai Zhou, shikai Li, Jingyun Liang, Chaohui Yu, Fan Wang, Xiangyang Xue, and Yanwei Fu. Uni3c: Unifying precisely 3d-enhanced camera and human motion controls for video generation. *arXiv preprint arXiv:2504.14899*, 2025. 2, 3, 4, 6, 7, 8
- [5] Haoxin Chen, Yong Zhang, Xiaodong Cun, Menghan Xia, Xintao Wang, Chao Weng, and Ying Shan. Videocrafter2: Overcoming data limitations for high-quality video diffusion models. In *CVPR*, pages 7310–7320. IEEE Computer Society, 2024. 3
- [6] Hao He, Yinghao Xu, Yuwei Guo, Gordon Wetzstein, Bo Dai, Hongsheng Li, and Ceyuan Yang. Cameractrl: Enabling camera control for text-to-video generation, 2025. 3, 7
- [7] Chen Hou and Zhibo Chen. Training-free camera control for video generation. In *ICLR*, 2025. 2, 3
- [8] Tao Hu, Haoyang Peng, Xiao Liu, and Yuewen Ma. Ex-4d: Extreme viewpoint 4d video synthesis via depth watertight mesh, 2025. 3
- [9] Jiahui Huang, Qunjie Zhou, Hesam Rabeti, Aleksandr Korovko, Huan Ling, Xuanchi Ren, Tianchang Shen, Jun Gao, Dmitry Slepichev, Chen-Hsuan Lin, Jiawei Ren, Kevin Xie, Joydeep Biswas, Laura Leal-Taixe, and Sanja Fidler. Vipe: Video pose engine for 3d geometric perception. *arXiv preprint arXiv:2508.10934*, 2025. 3
- [10] Ziqi Huang, Yanan He, Jiashuo Yu, Fan Zhang, Chenyang Si, Yuming Jiang, Yuanhan Zhang, Tianxing Wu, Qingyang Jin, Nattapol Chanpaisit, Yaohui Wang, Xinyuan Chen, Limin Wang, Dahua Lin, Yu Qiao, and Ziwei Liu. VBench: Comprehensive benchmark suite for video generative models. In *Proceedings of the IEEE/CVF Conference on Computer Vision and Pattern Recognition*, 2024. 2, 5, 7, 8, 1
- [11] Zeyinzi Jiang, Zhen Han, Chaojie Mao, Jingfeng Zhang, Yulin Pan, and Yu Liu. Vace: All-in-one video creation and editing, 2025. 2, 3, 4, 5, 7, 8
- [12] Xuan Ju, Weicai Ye, Quande Liu, Qiulin Wang, Xintao Wang, Pengfei Wan, Di Zhang, Kun Gai, and Qiang Xu. Fulldit: Multi-task video generative foundation model with full attention, 2025. 3
- [13] Nikhil Keetha, Norman Müller, Johannes Schönberger, Lorenzo Porzi, Yuchen Zhang, Tobias Fischer, Arno Knapitsch, Duncan Zauss, Ethan Weber, Nelson Antunes, Jonathon Luiten, Manuel Lopez-Antequera, Samuel Rota Bulò, Christian Richardt, Deva Ramanan, Sebastian Scherer, and Peter Kotschieder. Mapanything: Universal feed-forward metric 3d reconstruction. *arXiv preprint arXiv:2509.13414*, 2025. 3
- [14] Shenggui Li, Fuzhao Xue, Yongbin Li, and Yang You. Sequence parallelism: Making 4d parallelism possible. *CoRR*, abs/2105.13120, 2021. 6, 3
- [15] Zhiqiu Lin, Siyuan Cen, Daniel Jiang, Jay Karhade, Hwei Wang, Chancharik Mitra, Yu Tong Tiffany Ling, Yuhan Huang, Sifan Liu, Mingyu Chen, Rushikesh Zawat, Xue Bai, Yilun Du, Chuang Gan, and Deva Ramanan. Towards understanding camera motions in any video. 2025. 2, 5, 7, 8
- [16] Norman Müller, Katja Schwarz, Barbara Rössle, Lorenzo Porzi, Samuel Rota Bulò, Matthias Nießner, and Peter Kotschieder. Multidiff: Consistent novel view synthesis from a single image. In *Proceedings of the IEEE/CVF Conference on Computer Vision and Pattern Recognition (CVPR)*, pages 10258–10268, 2024. 2, 3
- [17] Stefan Popov, Amit Raj, Michael Krainin, Yuanzhen Li, William T. Freeman, and Michael Rubinstein. Camctrl3d: Single-image scene exploration with precise 3d camera control. In *2025 International Conference on 3D Vision (3DV)*, pages 649–658, 2025. 2, 3
- [18] Xuanchi Ren, Tianchang Shen, Jiahui Huang, Huan Ling, Yifan Lu, Merlin Nimier-David, Thomas Müller, Alexander Keller, Sanja Fidler, and Jun Gao. Gen3c: 3d-informed world-consistent video generation with precise camera control. In *CVPR*, 2025. 2, 3
- [19] Johannes L. Schönberger, Enliang Zheng, Jan-Michael Frahm, and Marc Pollefeys. Pixelwise view selection for unstructured multi-view stereo. In *ECCV*, pages 501–518, Cham, 2016. Springer International Publishing. 3
- [20] Junyoung Seo, Kazumi Fukuda, Takashi Shibuya, Takuya Narihira, Naoki Murata, Shoukang Hu, Chieh-Hsin Lai, Seungryong Kim, and Yuki Mitsufuji. Genwarp: Single image to novel views with semantic-preserving generative warping. *NeurIPS*, 37:80220–80243, 2024. 2, 3
- [21] Kuaishou Technology. Kling ai: Text-to-video generation from kuaishou. <https://klingai.com>, 2024. Accessed: 2025-11-05. 5, 2
- [22] Team Wan, Ang Wang, Baole Ai, Bin Wen, Chaojie Mao, Chen-Wei Xie, Di Chen, Feiwu Yu, Haiming Zhao, Jianxiao Yang, Jianyuan Zeng, Jiayu Wang, Jingfeng Zhang, Jingren Zhou, Jinkai Wang, Jixuan Chen, Kai Zhu, Kang Zhao, Keyu Yan, Lianghua Huang, Mengyang Feng, Ningyi Zhang, Pandeng Li, Pingyu Wu, Ruihang Chu, Ruili Feng, Shiwei Zhang, Siyang Sun, Tao Fang, Tianxing Wang, Tianyi Gui, Tingyu Weng, Tong Shen, Wei Lin, Wei Wang, Wei Wang, Wenmeng Zhou, Wenting Wang, Wenting Shen, Wenyuan Yu, Xianzhong Shi, Xiaoming Huang, Xin Xu, Yan Kou, Yangyu Lv, Yifei Li, Yijing Liu, Yiming Wang, Yingya Zhang, Yitong Huang, Yong Li, You Wu, Yu Liu, Yulin Pan, Yun Zheng, Yuntao Hong, Yupeng Shi, Yutong Feng, Zeyinzi Jiang, Zhen Han, Zhi-Fan Wu, and Ziyu Liu. Wan: Open and advanced large-scale video generative models. *arXiv preprint arXiv:2503.20314*, 2025. 2, 4, 5
- [23] Jianyuan Wang, Minghao Chen, Nikita Karaev, Andrea Vedaldi, Christian Rupprecht, and David Novotny. Vggt:

- Visual geometry grounded transformer. In *Proceedings of the IEEE/CVF Conference on Computer Vision and Pattern Recognition*, 2025. 2, 3, 4, 5, 8, 1
- [24] Xiang Wang, Hangjie Yuan, Shiwei Zhang, Dayou Chen, Jiniu Wang, Yingya Zhang, Yujun Shen, Deli Zhao, and Jinguang Zhou. Videocomposer: Compositional video synthesis with motion controllability. In *Advances in Neural Information Processing Systems*, pages 7594–7611. Curran Associates, Inc., 2023. 3
- [25] Yifan Wang, Jianjun Zhou, Haoyi Zhu, Wenzheng Chang, Yang Zhou, Zizun Li, Junyi Chen, Jiangmiao Pang, Chunhua Shen, and Tong He. π^3 : Scalable permutation-equivariant visual geometry learning. *arXiv preprint arXiv:2507.13347*, 2025. 3
- [26] Zun Wang, Jaemin Cho, Jialu Li, Han Lin, Jaehong Yoon, Yue Zhang, and Mohit Bansal. Epic: Efficient video camera control learning with precise anchor-video guidance, 2025. 3, 7
- [27] Zhuoyi Yang, Jiayan Teng, Wendi Zheng, Ming Ding, Shiyu Huang, Jiazheng Xu, Yuanming Yang, Wenyi Hong, Xiaohan Zhang, Guanyu Feng, Da Yin, Yuxuan Zhang, Weihang Wang, Yean Cheng, Bin Xu, Xiaotao Gu, Yuxiao Dong, and Jie Tang. Cogvideox: Text-to-video diffusion models with an expert transformer. In *ICLR*, 2025. 2, 3
- [28] Wangbo Yu, Jinbo Xing, Li Yuan, Wenbo Hu, Xiaoyu Li, Zhipeng Huang, Xiangjun Gao, Tien-Tsin Wong, Ying Shan, and Yonghong Tian. Viewcrafter: Taming video diffusion models for high-fidelity novel view synthesis. *arXiv preprint arXiv:2409.02048*, 2024. 2, 3
- [29] Liping Yuan, Jiawei Wang, Haomiao Sun, Yuchen Zhang, and Yuan Lin. Tarsier2: Advancing large vision-language models from detailed video description to comprehensive video understanding, 2025. 6
- [30] Liping Yuan, Jiawei Wang, Haomiao Sun, Yuchen Zhang, and Yuan Lin. Tarsier2: Advancing large vision-language models from detailed video description to comprehensive video understanding. *arXiv preprint arXiv:2501.07888*, 2025. 1, 2
- [31] Yabo Zhang, Yuxiang Wei, Dongsheng Jiang, XIAOPENG ZHANG, Wangmeng Zuo, and Qi Tian. Controlvideo: Training-free controllable text-to-video generation. In *ICLR*, 2024. 3
- [32] Rui Zhao, Yuchao Gu, Jay Zhangjie Wu, David Junhao Zhang, Jia-Wei Liu, Weijia Wu, Jussi Keppo, and Mike Zheng Shou. Motiondirector: Motion customization of text-to-video diffusion models. In *ECCV*, pages 273–290. Springer, 2024. 3
- [33] Yanli Zhao, Andrew Gu, Rohan Varma, Liang Luo, Chien-Chin Huang, Min Xu, Less Wright, Hamid Shojanazeri, Myle Ott, Sam Shleifer, Alban Desmaison, Can Balioglu, Pritam Damania, Bernard Nguyen, Geeta Chauhan, Yuchen Hao, Ajit Mathews, and Shen Li. Pytorch fsdp: Experiences on scaling fully sharded data parallel, 2023. 6, 3
- [34] Jensen (Jinghao) Zhou, Hang Gao, Vikram Voleti, Aaryaman Vasishtha, Chun-Han Yao, Mark Boss, Philip Torr, Christian Rupprecht, and Varun Jampani. Stable virtual camera: Generative view synthesis with diffusion models. *arXiv preprint*, 2025. 3, 7
- [35] Zhenghong Zhou, Jie An, and Jiebo Luo. Latent-reframe: Enabling camera control for video diffusion models without training. In *ICCV*, pages 12779–12789, 2025. 2, 3

CETCAM: Camera-Controllable Video Generation via Consistent and Extensible Tokenization

Supplementary Material

6. Phase I Training Data Filtering Details

This section provides the full details of the filtering pipeline used to construct the Phase I training dataset. Our goal is to obtain a large, diverse collection of raw Internet videos that exhibit meaningful camera motion, sufficient aesthetic quality, and reliable geometry estimates from VGGT [23]. Starting from an initial pool of approximately 330K crawled videos, the final filtered dataset contains about 100K clips. We obtain the captions of the training data from [30] and use them as prompts during Phase I training. We describe each filtering stage below.

6.1. Source Collection and Initial Preprocessing

We gather publicly accessible Internet videos covering a broad range of content types, including indoor and outdoor natural scenes, human–object interactions, cinematic B-roll, landscape footage, and casual handheld recordings. All videos are used in full accordance with their respective licenses, which permit research activities such as model training. We further verify that the dataset excludes all offensive, violent, or otherwise inappropriate material. No identity-specific content is intentionally collected. Each raw video undergoes the following preprocessing steps:

- **Frame extraction:** Frames are uniformly re-sampled at 16 FPS.
- **Resolution normalization:** The longer image side is resized to 720 pixels while preserving aspect ratio.
- **Clip segmentation:** Videos longer than 45 seconds are divided into 8–12 second clips via shot-boundary detection using HSV-gradient and color-histogram thresholds.
- **Discard rules:** Clips with effective resolution below 360p, severe compression artifacts, or fewer than 81 usable frames are removed.

This produces roughly 330K candidate clips for further filtering.

6.2. Camera Motion Detection with VGGT

Phase I training requires videos with visible camera motion rather than static-camera footage. For each clip, we apply VGGT [23] to estimate per-frame extrinsic parameters $\{\mathbf{E}_t\}_{t=1}^T$, where $\mathbf{E}_t = [\mathbf{R}_t | \mathbf{T}_t]$.

Translation and Rotation Magnitudes. We compute the frame-to-frame translation:

$$\Delta_T(t) = \|\mathbf{T}_{t+1} - \mathbf{T}_t\|_2, \quad (9)$$

and the quaternion-based rotation:

$$\Delta_R(t) = 2 \arccos(|\langle \mathbf{q}_{t+1}, \mathbf{q}_t \rangle|). \quad (10)$$

We use the mean values μ_T and μ_R as indicators of camera motion.

Static-Camera Rejection. A clip is removed if the motion magnitudes satisfy:

$$\mu_T < 0.002 \quad \text{and} \quad \mu_R < 0.5^\circ. \quad (11)$$

We additionally discard clips with discontinuous, unstable, or invalid pose predictions (e.g., quaternion flips, NaNs). After this step, approximately 160K clips remain.

6.3. Aesthetic Quality Filtering

To ensure the model does not learn low-quality photometric statistics, we evaluate each clip using the VBench [10] aesthetic quality predictor. For each frame:

$$s_{\text{aesthetic}} = \frac{1}{T} \sum_{t=1}^T f_{\text{VBench}}(I_t). \quad (12)$$

We discard clips with $s_{\text{aesthetic}} < 0.20$. Heuristic rules remove additional low-quality clips exhibiting excessive compression, over/underexposure, or artificial slideshow-like pan-zoom effects. This step removes approximately 60K clips.

6.4. Filtering Summary

Stage	Videos	Reduction
Raw crawled videos	330,421	–
Motion filtering	160,002	–52%
Aesthetic filtering	100,021	–38%

Table 3. Phase I training data filtering summary.

Table 3 summarizes the filtering pipeline. The final Phase I dataset thus offers stable and meaningful camera motion and high aesthetic quality, providing a strong foundation for learning robust and generalizable camera control.

7. HoIQ Benchmark Collection

This section provides details of how we construct the HoIQ benchmark used in Phase II training and all evaluations involving human–object interactions (HoI) and

high-fidelity indoor scenes. The goal of HoIHQ is to create a high-quality, diverse, and geometry-rich dataset that complements CameraBench [15] and Uni3C-OOD-Challenging [4]. All videos in HoIHQ are generated using the state-of-the-art commercial video foundation model Kling 2.5 [21], paired with carefully curated source images. The content focuses primarily on shopping-related scenarios with high commercial value. No real identity-specific content is included. Below, we describe each component in detail.

7.1. Source Image Collection

Our pipeline starts with constructing a diverse image corpus emphasizing human–object interactions (HoI) and indoor settings. All images are sourced from publicly accessible datasets and copyright-free photography repositories that permit research usage. To ensure strong geometric cues and compatibility with controllable video generation, we apply the following preprocessing and filtering steps:

- **Resolution requirement:** Images must have a minimum longer-side resolution of 720 px.
- **Foreground quality:** The main subject (human, object, or both) must be clearly visible, not heavily occluded, and free of motion blur.
- **Scene type diversity:** Images are selected across a broad set of categories including kitchen, living room, office, workshop, retail stores, and studio environments.
- **Safety filtering:** Images containing identifiable private individuals, minors, copyrighted characters, or sensitive content are manually removed.

A total of **500** high-quality HoI-focused images are preserved after filtering.

7.2. Prompt Generation

Before generating videos, we first construct a text prompt for each input image. Each prompt contains two components: a content description that captures the scene semantics, and a camera-movement instruction that specifies the intended motion. Both components are generated jointly using a Tarsier-2 [30]. We feed the image into Tarsier-2 and, through carefully designed system instructions, ask the model to produce a prompt that (1) accurately reflects the visual content—especially human–object interaction, (2) includes plausible rich motion movements, (3) includes explicit, large-scale camera-movement directives. This design encourages the model to learn strong and diverse camera motions in the resulting training videos. Here we provide some sample prompts used to generate videos:

- **Sample Prompt 1.** Camera: wide orbit left with extreme dolly out. Outdoors, captured in a medium shot, a woman stands near the ocean, holding a phone with a stylish case in her hand. The background features soft waves and a cloudy sky, creating a serene coastal vibe. She gently

raises the phone to eye level, showcasing the case’s design while maintaining a natural and relaxed posture. The overall atmosphere is calm and breezy, complementing the coastal setting.

- **Sample Prompt 2.** Camera: wide orbit right with extreme dolly in. Outdoors, captured in a bright, sunny medium shot, a woman sits poolside holding a sunscreen spray bottle. She gently sprays the product onto her leg and spreads it evenly, highlighting the ease of application and smooth texture. The scene conveys a carefree, summery mood, enhanced by the sparkling pool in the background.
- **Sample Prompt 3.** Camera: extreme dolly out with sweeping pan left. Indoors, captured in a medium shot, a child wearing a bright yellow sweater sits at a table with a glass of chocolate drink in front of them. The child picks up the glass with both hands and takes a sip, emphasizing the drink’s creamy texture. The vibrant blue background and cheerful setting reinforce a playful and inviting atmosphere.

7.3. Video Generation Using Kling 2.5 [21]

For each source image and each prompt with camera, we generate a 5-second video using the Kling 2.5 video generation model. Kling 2.5 is chosen due to its strong scene coherence, high-resolution synthesis, and stable handling of indoor scenes. Each video cost about five US dollars. The generation protocol is standardized to maintain reproducibility:

- **Input:** See Section 7.1.
- **Prompt:** See Section 7.2.
- **Model Settings:** 16 FPS, 5-second duration, default Kling sampling schedule.

We generated a dataset of 500 videos. The dataset is randomly split into two parts, where 100 videos are left for evaluation, while the remaining videos are used for training.

8. Quantitative Comparison against VACE

To evaluate the extensibility of CETCAM beyond camera control, we conduct a detailed quantitative comparison against the unified controllable video generation framework VACE [11]. We benchmark both methods across four representative controllable-generation tasks: inpainting, gray-to-color, scribble-to-video, and reference-image conditioning. Source videos, prompts and videos are from the VACE benchmark. For each task, we report VBench scores (overall, consistency, aesthetic quality, imaging quality, temporal stability, and motion smoothness), 3D camera metrics (ATE/RPE/RRE), and two-part human evaluation: *Human-Gen* for overall perceptual quality and *Human-Cam* for perceived camera-following accuracy and smoothness. When grading *Human-Cam*, human participants are given a de-

Method	Overall	Subject	Background	Aesthetic	Imaging	Temporal	Motion	ATE↓	RPE↓	RRE↓	Human-Gen↑	Human-Cam↑
Task: Inpainting												
VACE [11]	84.91	89.34	92.17	61.42	71.33	98.14	97.28	3.912	1.942	14.21	91.2	12.3
CETCAM (Ours)	86.73	91.26	93.51	59.31	73.28	97.93	99.41	0.812	0.301	3.674	92.8	89.6
Task: Gray-to-Color												
VACE [11]	85.77	90.54	92.83	60.74	70.08	97.56	96.95	3.504	1.721	12.92	92.0	10.7
CETCAM (Ours)	86.12	91.04	93.08	58.91	72.74	97.85	99.44	0.793	0.286	3.622	91.9	90.4
Task: Scribble-to-Video												
VACE [11]	84.62	89.03	91.04	57.64	69.08	97.61	96.22	4.221	2.104	15.01	90.7	11.8
CETCAM (Ours)	85.57	90.52	92.64	57.83	71.30	97.44	99.10	0.864	0.319	3.811	91.4	88.7
Task: Reference Image												
VACE [11]	86.92	91.71	94.33	61.12	71.21	97.86	97.44	3.712	1.863	14.83	93.1	13.9
CETCAM (Ours)	87.24	92.81	93.57	58.62	76.02	98.06	99.58	0.768	0.259	3.414	93.4	92.7

Table 4. **Extensibility comparison between VACE and CETCAM across four compositional control tasks.** VACE achieves competitive or even stronger VBench scores in a few dimensions (e.g., aesthetic quality, temporal stability, or background consistency). However, VACE completely fails at camera-following, resulting in extremely poor pose metrics and Human-Cam scores. CETCAM maintains competitive generation quality while delivering accurate and smooth 3D-consistent camera control across all tasks.

scription of the input camera trajectory. Other settings are same as specified before in Section 4.3.

Table 4 shows that VACE achieves competitive—and occasionally higher—VBench scores on appearance-centric metrics such as aesthetic quality, temporal stability, or background consistency. This reflects its strong underlying video diffusion backbone and its ability to perform high-quality appearance editing under various conditioning modalities. However, VACE fundamentally lacks camera-following capability. Since its architecture does not incorporate explicit geometry grounding or pose-dependent conditioning, VACE produces videos that visually resemble the controlled input but do not track the prescribed camera trajectory. This results in extremely poor pose accuracy across all tasks, with ATE, RPE, and RRE one to two orders of magnitude worse than CETCAM. The Human-Cam evaluation confirms this failure: participants consistently rated VACE’s camera adherence as very low (~ 10 – 14), often reporting “static-camera” or “incorrect motion” artifacts. In contrast, CETCAM maintains strong and consistent performance across both appearance and geometry domains. Overall, CETCAM offers the best of both worlds: competitive generation quality and reliable camera-following behavior. Meanwhile, VACE remains effective as a general-purpose controllable generator but is fundamentally unsuitable for camera-based control due to its absence of 3D-consistent mechanisms.

9. Model Parallelization Details.

To save GPU memory, we implement two essential strategies: Fully Sharded Data Parallel (FSDP) [33] and Sequence Parallelism (SP) [14]. These two techniques are applied on the base Wan DiT blocks, not on the CETCAM Context Blocks or VACE Context Blocks. FSDP [33] par-

titutions model parameters, gradients, and optimizer states across multiple GPUs, substantially reducing per-device memory usage while preserving scalability. We enable mixed precision with `bf16` computation to further reduce activation memory. SP [14] further distributes long sequence computations among devices, allowing efficient handling of large spatiotemporal token sequences during training. We use a SP size of two during our training.